A NOVEL METHOD FOR COMPUTING THE VERTICAL GRADIENTS OF THE POTENTIAL FIELD: APPLICATION TO DOWNWARD CONTINUATION

Tran Van Kha[1], Nguyen Nhu Trung[1,2 *]

[1] Institute of Marine Geology and Geophysics, VAST, 18 Hoang Quoc Viet, Hanoi, Vietnam.

[2]Graduate University of Science and Technology, VAST.

* Corresponding author's email: nntrung@imgg.vast.vn

Abstract: Downward continuation is a very useful technique in the interpretation of potential field data. It would enhance the short wavelength of the gravity anomalies or accentuate the details of the source distribution. Taylor series expansion method has been proposed to be one of the best downward continued methods. However, the method using high-order vertical derivatives leads to low accuracy and instability results in many cases. In this paper, we propose a new method using a combination of Taylor series expansion and upward continuation for computing vertical derivatives. This method has been tested on the gravitational anomaly of infinite horizontal cylinder in both cases with and without random noise for higher accurate and stable than Hilbert transform method and Laplace equation method, especially in the case of noise input data. This vertical derivative method is applied successfully to calculate the downward continuation according to Taylor series expansion method. The downward continuation is also tested on both complex synthetic models and real data in the East Vietnam Sea (South China Sea). The results reveal that by calculating this new vertical derivative, the downward continuation method gave higher accurate and stable than the previous downward continuation methods.

Keyword: Gravity anomalies and earth structure, numerical approximations and analysis, Asia, geopotential theory, satellite gravity, structure of the Earth.

INTRODUCTION

Downward continuation is a useful method in the processing and interpretation of potential field data. When the observed stations are required to be close to the field sources for enhancing the short wavelength of the potential field anomalies, further downward continuation can be applied. However, downward continuation of potential fields is intrinsically unstable and divergent because of the following reasons: a field at lower elevation from a higher elevation cannot be obtained directly (Parker, 1977, Tikhonov et al., 1977, Sansó et al., 2018), and if downward continuation encounters an exceptional source, oscillation occurs (Fedi and Florio, 2002). The downward continuation will greatly amplify the shortest wavelength of the measured data to a degree that depends on the downward continuation distance (Δh) and the sampling interval of the data (Blakely, 1996, p. 320). For the purpose of making downward continuation stable and accurate, geophysicists have proposed several different methods (Clarke, 1969; Tikhonov et al., 1977; Huestis & Parker, 1979; Ferguson, 1988; Pawlowski, 1995; Fedi and Florio, 2002; Cooper, 2004, Xu *et al.*, 2007; Pašteka et al., 2012; Abedi et al., 2013; Lima et al., 2013; Sebera et al., 2014, 2015; Zhang et al., 2013, 2016, Mansi et al., 2018). Thus far, three methods for calculating the downward continuation have been proposed. First method involves the downward continuation using the inverse calculation based on the Dirichlet integral formula in the spatial domain (Bullard & Cooper, 1948; Achache et al., 1987; Morgan & Blackman, 1993; Mastellone et al., 2013). The major disadvantages of this method are that it provides multiple solutions to a problem and the calculation process is unreliable (Novák et al., 2001; Fedi& Florio, 2002). The second method uses a linear multiplication algorithm based on the convolution in the frequency domain (Tsuboi & Fuchida, 1937; Hughes, 1942; Tomoda & Aki, 1955; Dean, 1958). This method needs to filter the frequency downward continuation

factor to reduce the amplified impact and implement appropriate methods to diminish the border effect (Clarke, 1969; Tikhonov et al., 1977; Huestis & Parker, 1979; Ferguson, 1988; Pawlowski, 1995; Pašteka et al., 2012; Abedi et al., 2013; Lima et al., 2013; Sebera et al., 2015; Zhang et al., 2016). The third method uses Taylor series expansion via potential field and its different order derivative values (Evjen, 1936; Peters, 1949; Trejo, 1954; Ackerman, 1971; Cooper 2004; Zhang et al., 2013; Abedi et al., 2013). The major disadvantage of this method includes the requirement of multiple-step iteration calculation; also, the method for calculating the vertical derivatives in different orders is not clear (Fedi and Florio, 2001, Zhang et al., 2013). Recently, Zhang et al., (2018) used a numerical solution of the mean value theorem to overcome the instability and inaccuracy of the downward continuation method for a potential field. However, this method has a limitation. It is necessary to use the vertical derivatives directly measured in the potential field; thus, the method is only effective in places where the vertical derivatives of the real data are available.

In this article, we present a new method of calculating the vertical derivatives with high accuracy and stability. The new vertical derivative method uses a combination of the Taylor series expansion and the upward continuation for establishing matrix equations that represent the relation between vertical derivatives of the field ($\partial f(x, y, z) / \partial z$, $\partial^2 f(x, y, z) / \partial^2 z$, ..., $\partial^n f(x, y, z) / \partial^n z$) and their field values at higher elevations $n\Delta h$ ($f(x, y, z - \Delta h)$, $f(x, y, z - 2\Delta h)$, ..., $f(x, y, z - n\Delta h)$, n=1, 2, 3…N). The potential field at higher elevations can be obtained by the upward continuation method which is a smoothing operation. The new vertical derivative method is applied successfully to downward continuation method and demonstrated efficiently its application to synthetic models and real data.

1- Theoretical basis and calculation method

Assuming the function f (x, y, z) is any potential field measured at height z (gravity or magnetic fields), the Cartesian coordinate system is used, the positive z-axis points vertically downwards, and the function f(x, y, z+Δh) at position (z+Δh) can be expressed by Taylor series expansion as follows (Peter, 1949, Fedi and Florio, 2002):

$$f(x,y,z+\Delta h) = f(x,y,z) + \Delta h f'(x,y,z) + \frac{(\Delta h)^2}{2!} f''(x,y,z) + \cdots + \frac{(\Delta h)^n}{n!} f^n(x,y,z) \qquad (1)$$

where $f'(x,y,z), f''(x,y,z), \ldots, f^n(x,y,z)$ are the vertical derivative of orders 1, 2, 3,… N of function f(x, y, z); and Δh is the distance of downward continuation. To determine the value f(x, y, z+Δh) we need to determine the vertical derivative (VD) $f'(x,y,z), f''(x,y,z), \ldots, f^n(x,y,z)$. The key issue in formula (1) is how to calculate the vertical derivative of orders 1, 2, 3, …, N. In this article, we do not define the vertical derivative values by the FFT method; we propose a new method to define them through the upward continuation values (f (x, y, z - Δh), f (x, y, z - 2Δh), ... f (x, y, z - nΔh)). Using this method, the vertical derivatives obtained are stable and accurate. Indeed, we consider the Taylor series expansion of n = 1, 2, 3, ..., N; Δh is small enough and positive, and we have the following equation system:

$$\begin{cases} f(x,y,z-\Delta h) = f(x,y,z) - \Delta h f'(x,y,z) + \dfrac{(-\Delta h)^2}{2!} f''(x,y,z) + \ \ldots\ + \dfrac{(-\Delta h)^n}{n!} f^n(x,y,z) \\ f(x,y,z-2\Delta h) = f(x,y,z) - 2\Delta h f'(x,y,z) + \dfrac{(-2\Delta h)^2}{2!} f''(x,y,z) + \cdots + \dfrac{(-2\Delta h)^n}{n!} f^n(x,y,z) \\ \quad\vdots \\ f(x,y,z-n\Delta h) = f(x,y,z) - n\Delta h f'(x,y,z) + \dfrac{(-n\Delta h)^2}{2!} f''(x,y,z) + \cdots + \dfrac{(-n\Delta h)^n}{n!} f^n(x,y,z) \end{cases} \qquad (2)$$

where $f(x,y,z-\Delta h), f\left(x,y,z-2\Delta h,\ldots,f(x,y,z-n\Delta h)\right)$ are the upward continuations at distances of Δh, 2Δh, 3Δh,… nΔh.

Equation (2) can be rewritten as the matrix equation:

$$\begin{pmatrix} -\Delta h & \frac{(-\Delta h)^2}{2!} \ldots & \frac{(-\Delta h)^n}{n!} \\ -2\Delta h & \frac{(-2\Delta h)^2}{2!} \ldots & \frac{(-2\Delta h)^n}{n!} \\ & \vdots & \\ -n\Delta h & \frac{(-n\Delta h)^2}{2!} \ldots & \frac{(-n\Delta h)^n}{n!} \end{pmatrix} \begin{pmatrix} f'(x,y,z) \\ f''(x,y,z) \\ \vdots \\ f^n(x,y,z) \end{pmatrix} = \begin{pmatrix} f(x,y,z-\Delta h)-f(x,y,z) \\ f(x,y,z-2\Delta h)-f(x,y,z) \\ \vdots \\ f(x,y,z-n\Delta h)-f(x,y,z) \end{pmatrix} \quad (3)$$

Solving the linear Equation (3), we get $f'(x,y,z), f''(x,y,z), \ldots f^n(x,y,z)$ and by substituting them into Equation (1), we obtain the downward continuation $f(x,y,z+\Delta h)$ formula as follows:

$$f(x,y,z+\Delta h) = a_0 f(x,y,z) + a_1 f(x,y,z-\Delta h) + a_2 f(x,y,z-2\Delta h) + a_3 f(x,y,z-3\Delta h) + \cdots + a_4 f(x,y,z-4\Delta h) + a_5 f(x,y,z-5\Delta h) + \cdots + a_n(x,y,z-n\Delta h) \quad (4)$$

where a_0, a_1, ..., a_n are the values determined from solving Equation (3) corresponding to the order n in the Taylor series expansion. For example, n = 3, Equation (1) becomes:

$$f(x,y,z+\Delta h) = f(x,y,z) + \Delta h f'(x,y,z) + \frac{(\Delta h)^2}{2!} f''(x,y,z) + \frac{(\Delta h)^3}{3!} f'''(x,y,z) \quad (5)$$

and Equation system (2) becomes:

$$\begin{cases} f(x,y,z-\Delta h) = f(x,y,z) - \Delta h f'(x,y,z) + \frac{(-\Delta h)^2}{2!} f''(x,y,z) + \frac{(-\Delta h)^3}{3!} f'''(x,y,z) \\ f(x,y,z-2\Delta h) = f(x,y,z) - 2\Delta h f'(x,y,z) + \frac{(-2\Delta h)^2}{2!} f''(x,y,z) + \frac{(-2\Delta h)^3}{3!} f'''(x,y,z) \\ f(x,y,z-3\Delta h) = f(x,y,z) - 3\Delta h f'(x,y,z) + \frac{(-3\Delta h)^2}{2!} f''(x,y,z) + \frac{(-3\Delta h)^3}{3!} f'''(x,y,z) \end{cases} \quad (6)$$

Solving the linear Equation system (6), we get $f'(x,y,z), f''(x,y,z), f'''(x,y,z)$ as follows (Appendix A):

$$f'(x,y,z) = \frac{11f(x,y,z) - 18f(x,y,z-\Delta h) + 9f(x,y,z-2\Delta h) - 2f(x,y,z-3\Delta h)}{6\Delta h} \quad (7)$$

$$f''(x,y,z) = \frac{2f(x,y,z) - 5f(x,y,z-\Delta h) + 4f(x,y,z-2\Delta h) - f(x,y,z-3\Delta h)}{\Delta h^2} \quad (8)$$

$$f'''(x,y,z) = \frac{f(x,y,z) - 3f(x,y,z-\Delta h) + 3f(x,y,z-2\Delta h) - f(x,y,z-3\Delta h)}{\Delta h^3} \quad (9)$$

Substituting Equations (7), (8) and (9) into Equation (5), we obtain the downward continuation $f(x,y,z+\Delta h)$ formula as follows:

$$f(x,z+\Delta h) = 4f(x,y,z) - 6f(x,y,z-\Delta h) + 4f(x,y,z-2\Delta h) - f(x,y,z-3\Delta h) \quad (10)$$

where $a_0 = 4$; $a_1 = -6$, $a_2 = 4$; $a_3 = -1$

Table 1 shows the values of a_0, a_1, ..., a_n in cases where n = 3, 5, 8, and 10.

It can be seen that the calculation of the downward continuation is determined by the upward continuation values of function f(x, y, z) at different distances ($\Delta h,\ 2\Delta h, \ldots, n\Delta h$). As stated, the upward continuation is a smooth operation and provides stable and accurate results (Blakely, 1995, p. 319). If we continue downward to a distance h (h = mΔh, m = 1, M), the upward continuation is calculated to N different distances. Substituting Δh by mΔh into Equation (4), we obtain the general formula of the downward continuation $f(x,y,z+m\Delta h)$ as follows:

$$f(x,y,z+m\Delta h) = a_0 f(x,y,z-(1-m)\Delta h) + a_1 f(x,y,z-(2-m)\Delta h) + a_2 f(x,y,z-(3-m)\Delta h) + a_3 f(x,y,z-(4-m)\Delta h) + \ldots + a_n f(x,y,z-(n+1-m)\Delta h). \quad (11)$$

The Equation (11) is coded with the order n =8 for computing the downward continuation in this article (Appendix B).

Error in calculating vertical derivatives (VD): In order to formulate (11), the main problem is the calculation of the first, second, third, ... n order VD of the function f (x, y, z). The

accuracy of these VD will determine the accuracy of the downward continuation formula. Hilbert transform method or Laplace equation method has been used to calculate these VD (Juan H.H. and Kenvin L.M., 2002, Ramadass et al., 1987, Fedi and Florio, 2002). However, one of the limitations of Hilbert transform and Laplace equation methods is that higher order VD is calculated from the previous order VD. Therefore, the error of calculating the VD is strongly affected by the error of the previous VD, especially when the input data is of poor quality. In our calculation method, the VD is calculated directly from the original field data f(x, y, z) and its upward continuation values. It does not depend on the result of the calculation of the previous VD (see equations (7), (8), (9)). Figure 1 and Table 2 compares the results of the calculation of the first, second, third and fourth order VD of the gravity anomaly of an infinite horizontal cylinder (with its diameter = 1 km, density 0.25 g/cm^3, located at 4.0001 km deep and grid point interval 0.25 km) by Hilbert transform, Laplace equation and our methods with the theoretical VD. We find that the root mean square (RMS) errors of the Hilbert transform and Laplace equation methods are larger than that of our method (Table 2). Especially when adding 5% random noises to the input data, the errors of Hilbert transform and Laplace equation methods are even much greater (Fig. 2 and Table 3). For example, their error of the third order VD is 11-17 times higher than our method, or 47 times in the case of the fourth order VD.

The computation requirement of the method: The equation system (2) has high accurate solution when a suitable Δh is chosen. The accuracy of the downward continuation could be affected by Δh value and the choice of Δh depends on the noise and the sampling interval of the input data (Blakely, 1995, p. 320). The larger the noise data, the larger is Δh chosen; the smaller the measured grid data, the smaller is Δh chosen. As a rule of thumb, Δh value is chosen as 0.5 to 1.5 times that of the measured grid data according to the data quality. In case of high noise data, the Δh value is chosen as larger two times of grid data.

The order of the Taylor series: A simple rule is that the simpler the model, the lower is the order of the Taylor transform chosen. In the case of a simple model, the order of the Taylor transform is chosen by 3 or 4 and in the case of a more complicated model, the larger n is chosen. However, the order n of the Taylor series expansion is usually chosen by 8 or 10 for most cases.

The equation system (2) are built directly from the origin measured data f(x, y, z) and its upward continuation. In case, the measured data have good quality, the calculation procedure of the formula (11) in Fig. B1 can skip the upward continuation step. For example, in the case of the correct input data in Fig. 1, we calculated directly the vertical derivative from the theoretical gravity anomaly, it does not need to upward continue and the calculation error is still small. In fact, gravity anomaly measured data will contain a certain error or noise; thus, in order to get a more stable and accurate downward continuation, the upward continuation can be applied to a certain distance to smooth the data before calculating the downward continuation according to Equation (11). For example, the VD are calculated directly from the 5% noise input data, the RMS errors are presented in Fig. 2 and Table 3. In the case, we upward continue the noise input data before calculating the downward continuation according to Equation (11), we get the first, second, third, and fourth VD that have smaller errors than the case without upward continuing (Table 3 and Table 4).

3. **Downward continuation of gravity anomaly of the synthetic models**

To demonstrate the effectiveness of our method, we used gravity anomalies of synthetic 2D and 3D models for calculating downward continuation and compared them with the theoretically calculated results and some other downward continuation methods.

2D synthetic model: Figure 3 shows a simple 2D synthetic model consisting of three rectangular bodies placed side by side with geometric and density parameters shown in Table 5. The first block is the largest and has highest density contrast with the surrounding rock.

The ratio of the width to the depth of the body is 15/4.1. It is the major contributor to the anomalies in gravity. The second and third bodies are smaller in size with lower density compared to the first one. The grid point interval of stations is 0.25 km. The synthetic gravity anomalies are calculated for two cases: with noise and without noise. The simple mirror technique is applied in the calculation procedure to diminish the border effect (Appendix B). In Fig. 3b, the theoretical gravity anomaly at z = 0 km (black line) mainly reflects the first block; the second and third bodies are almost invisible. The blue line represents the theoretical gravitational anomalies at z = 4 km of all three objects. The red, green and violet lines represent the downward continuation gravity anomalies at z = 4 km by our method, Zhang et al.'s method (Zhang el al., 2018) and Laplace Equation (Fedi et al., 2002), respectively. Fig. 3b and 1c show that our results are very stable and accurate, and very similar to the theoretical gravity anomalies as well as the results obtained by Zhang et al. (2018) and Fedi el al., (2002). The root mean square error of our method is 0.11 mGal (Table 6). If we add 5% random noise to synthetic gravity anomalies at z = 0 km (black line in Fig. 3d), the result of the downward continuation at z = 4 km indicate that our results are still very stable and accurate, while those obtained by Zhang et al.'s and Fedi et al.'s methods show some noises in the peak area of the anomaly. The RMS errors of our method and Zhang's method is similar, while the RMS errors of Fedi et al.'s method is very large (Table 6 and Fig. 3e).

Synthetic three-dimensional model: Figure 4 shows the 3D model consisting of three rectangular prisms placed side by side with geometric and density parameters presented in Table 7 (Fig. 4a and Fig. 4b). The 3D model is slightly more complicated than the 2D model in that the ratio between the width and the depth of the prism is 0.4 to 0.7 times smaller in the former. The grid intervals of stations are 0.1 × 0.1 km. Fig. 4c shows the gravity anomalies calculated at the observation surface z = 0 km. It seems to display only one big block;

however, but in fact, it shows three separate blocks. Theoretical gravity anomalies at the surface z = 1 km are presented in Fig. 4d. It clearly shows the anomalies of the three blocks. In Fig. 4e, gravity anomalies that continue downward at z = 1 km according to Zhang et al.'s method (2018) is depicted. Its anomalous shape resembles that of the theoretical anomalies in Fig. 4d. However, the magnitude of Zhang et al. 's anomalies was lower than the theoretical anomalies, especially in their extreme areas. Fig. 4g shows the residual error between Zhang et al.'s downward continued gravities (Fig. 4e) and the theoretical gravity anomalies (Fig. 4d). It shows that the residual error is very high, ranging from −1 to −0.7 mGal and 0.4 to 0.5 mGal around the maximum area. Fig. 4f represents the gravity anomalies that are continued downward at z = 1 km, according to Equation (11) with the order n = 8 in the Taylor series expansion (Appendix B), and the downward continuation distance Δh = 0.22 km and almost coincide with its theoretical gravity (Fig. 4e). The residual error between our downward continuation gravity (Fig. 4f) and the theoretical gravity anomalies (Fig. 4e) is very small in the maximum gravity anomaly area and nearly zero away from these areas (Fig. 4h). Fig. 4i shows the line BB' passing through the top of the object and displays Zhang et al.'s downward continued anomaly (blue line) and our downward continued gravity (red line). It shows that the former is much lower than its theoretical value (green line) of 0.95 mGal with the maximum gravity anomaly being 3.4 mGal. Our downward continued gravity anomalies were found to be very close to its theoretical values.

2- Application to downward continuation of the gravity anomaly of the Southwest Sub-basin, East Vietnam Sea (South China Sea)

The Southwest Sub-basin (SWSB) is a typical V-shaped oceanic basin of a propagating rift (Briais et al., 1993; Huchon et al., 2001; Li et al., 2013) located in the southwest of the Central Oceanic Basin, East Vietnam Sea (Fig. 5). The SWSB covers an area of approximately 130,000 km^2. Seafloor topography is fairly uniform with an average water

depth of 4203.3 m. The SWSB originated as a rift basin during late to Middle Miocene and was controlled mainly by the NW-SE Sea opening from 23.6 to 16 Ma (Chun-Feng Li et al, 2014, Briais et al., 1993). Owing to the impacts of polycyclic rifting, the SWSB was formed by events such as depressions and uplifts, seamounts, and buried volcanoes (Sandwell et al., 2009, 2014, Sandwell and Smith, 1997, Nguyen et al., 2004). Because the seafloor is very deep, gravity anomaly on the sea surface in the SWSB may not display or poorly display the small geological structures; therefore, it is difficult to interpret the gravity data or magnetic data.

It is good idea if we continue downward gravity anomaly data from sea surface to near the seabed level aiming at increasing the resolution of the marine gravity anomaly. The gravity anomaly data used in this section are obtained from the extract topography or gravity database available at https://topex.ucsd.edu/cgi-bin/get_data.cgi, (Sandwell et al., 2014, Sandwell et al., 2013). The data include 1 × 1 min grid of the satellite-derived free-air gravity, version 24.1. Figure 5b shows the Bouguer gravity anomaly of the SWSB obtained from calculating the complete Bouguer correction of the satellite-derived free-air gravity anomaly with the seawater density of 1.03 g/cm^3 and the typical crust density of 2.0 g/cm^3. To test the stability and accuracy of our downward continuation method for the real data, we conducted the upward continuation of the gravity anomalies (Fig. 5b) to 4 km to obtain the data represented in Fig. 5c. The data presented in this figure was considered the initial gravity anomaly data to calculate the downward continuation at z = 0 km by our method; these were further compared with the real anomalies (Fig. 5b). The obtained result of downward continuation (Fig. 5c) to 0 km (Fig. 5d) is stable and fit well with the real data (Fig. 5b). The residual error (Fig. 5e) between the downward continuation (Fig. 5d) and the real data (Fig. 5b) is very small, confirming the reliability and stability of our method. We continue the downward gravity anomaly (Fig. 5b) at z = 4 km (Fig. 5f) using our method. The gravity anomaly of downward continuation at z = 4 km is nearly the same as the original gravity

anomaly before continuing downward. However, it amplifies the range of the anomaly; some small-scale structures are visible and better displayed in the downward continued gravity anomaly. The seismic section VN08-14 (Fig. 5g and Fig. 5h) is used to compare the gravity anomaly on the sea surface and downward continuation gravity at z = 4 km and z = 5 km. Gravity anomalies on the sea surface (black line) show a relatively good reflection of main geological structures that are displayed in seismic section (Fig. 5h). However, some of the interfered structural blocks are not clearly shown. The gravity anomalies are continued downward at z = 4 km (red line) and 5 km (green line), and are amplified in the range of the short wavelength anomalies. Some of positive or negative geological structures shown in the seismic section are not visible on the gravity anomaly at z = 0 (sea surface), but they can be seen clearly in downward continuation gravity anomalies at z = 4 km and 5 km. For example, two seamounts at 165–175 km distance in the seismic section VN08-14 (Fig. 5h) are displayed on the sea surface gravity anomalies with a maximum gravity anomaly only; however, they are clearly reflected in gravity anomalies at z = 4 and z = 5 km as two anomalous peaks. We also find that the downward continued gravity anomalies at z = 4 and z = 5 km reflect the rugged basement better than the gravity anomalies at z = 0 km.

CONCLUSIONS

Based on the combination of the Taylor series expansion and upward continuation methods at different distances, we proposed a new method for computing the vertical derivatives. The proposed method was tested on the gravity anomaly of the infinity horizontal cylinder to yield higher accuracy and stability than the Hilbert transform and Laplace equation methods. The new vertical derivative method was applied successfully to downward continuation according to Taylor series expansion. The downward continuation was also applied on synthetic complex models and real data to yield stability, convergence, and high accuracy. The results show that the downward continuation is highly effective in increasing useful

signals. Moreover, small-sized objects are made clearer. Even for the noise gravity data, the downward continuation still depicted high stability and accuracy.

ACKNOWLEDGEMENTS

This research is funded by Vietnam National Foundation for Science and Technology Development (NAFOSTED) under grant number 105.99-2017.318. The authors thank honestly NAFOSTED.

APPENDIX A: MATLAB COMPUTER CODE FOR SOLVING LINEAR EQUANTIONS (FOR N=3)

```
%%%%%    CODE MATLAB FOR SOLVING LINEAR EQUANTIONS (FOR N=3)
%%%%%      f1, f2, f3 are the first, second and third vertical derivates,
respectively.
%%%%%   h is distance of upward continuation
%%%%%   uc0 is gravity anomaly
%%%%%   uc1 : upward continued gravity anomaly at distance z = -h
%%%%%   uc2 : upward continued gravity anomaly at distance z = -2h
%%%%%   uc3 : upward continued gravity anomaly at distance z = -3h
%%%%%%%%%%%%%%%%%%%%%%%%%%%%%%%%%%%%%%%%%%%%%%%%%%%%%%%%%%%%%%%%%%%%%%%%%%%%%%%
syms uc0 uc1  uc2 uc3 f1 f2 f3 h
eq1='-h*f1+(-h)^2/factorial(2)*f2+(-h)^3/factorial(3)*f3+uc0= uc1';
eq2='-2*h*f1+(-2*h)^2/factorial(2)*f2+(-2*h)^3/factorial(3)*f3+uc0= uc2';
eq3='-3*h*f1+(-3*h)^2/factorial(2)*f2+(-3*h)^3/factorial(3)*f3+uc0= uc3;
eq=solve(eq1,eq2,eq3,'f1','f2','f3');
f1=eq.f1
f2=eq.f2
f3=eq.f3
%%%%%%%%%%%%%%%%%%%%%%%%%%%%%%%%%%%% end program
```

APPENDIX B: MATLAB COMPUTER CODE FOR DOWNWARD CONTINUATION BY THIS ARTICLE, N = 8 IN TAYLOR SERIES EXPANSION (FOR FIG. 4F)

```
%%%%%%%%%%%%%%%%%%%%%%%%%%%%%%%%%%%%%%%%%%%%%%%%%%%%%%%%%%%%%%%%%%%%%%%%%%%%%%%
%%%%% MATLAB CODE FOR COMPUTING DOWNWARD CONTINUATION
%%%%%  N=8     : number of series Taylor
%%%%%  nx, ny  : number of points on the observation plane
%%%%%  dx, dy  : The grid intervals of stations (0.1 × 0.1 km)
%%%%%  Up      : distance of upward continuation
%%%%%  h       : distance of downward continuation
%%%%%  z       : the depth of downward continuation z = 8*h)
%%%%%  nn      : the number of calculation of upward continuation (nn=N=8)
%%%%%  G       : gravity anomalies at observation plane
%%%%%  UC0, UC1, UC2,...,UC8: are upward continued gravity anomalies at
%%%%%           distance -h, -2h,...-8h, respectively;
%%%%%  Grav_DC : downward continuation of gravity anomaly at distance z
%%%%%  model2.txt: input file data
```

```
clear all;close all;clc;
file=input('file data','s');
A=importdata(file);
G=A(1:end,3);x1=A(1:end,1);y1=A(1:end,2);
nx=128;ny=128;
dx=0.1;dy=0.1;
Up=0.1;z=1;h=0.22;
nn=(z+Up)/h;
l=0;
for i=1:nx
    for j=1:ny
        l=l+1;
        G3(i,j)=G(l);
        x(i,j)=x1(l);
        y(i,j)=y1(l);
    end
end
%%%%%%%%%%%%%%% Extend matrix data
GG1=repmat(G3(1,1:end),nx/2,1);
GG2=repmat(G3(end,1:end),nx/2,1);
GG5=[GG1;G3;GG2];
GG3=repmat(GG5(1:end,1),1,ny/2);
GG4=repmat(GG5(1:end,end),1,ny/2);
GG6=[GG3 GG5 GG4];
%%%%%%%%%%%%%%%%%%%%%%%%%%%%%%%%
m=nx+nx;n=ny+ny;
npts1=m;
npts2=n;
dkx1  = 2.0*pi/(npts1*dx);
dky1  = 2.0*pi/(npts2*dy);
nyqx = (npts1/2)+1;
nyqy = (npts2/2)+1;
for I=1:npts1
 for J=1:npts2
     if I<nyqx
  freqx(I,J)=(I-1)*dkx1;
     else
     freqx(I,J)=(I-npts1-1)*dkx1;
     end
     if J<nyqy
  freqy(I,J)=(J-1)*dky1;
     else
     freqy(I,J)=(J-npts2-1)*dky1;
     end
  freq(I,J)=sqrt(freqx(I,J)*freqx(I,J)+freqy(I,J)*freqy(I,J));
 end;
end;
Emu01=exp(-freq*h);
Emu02=exp(-freq*2*h);
Emu03=exp(-freq*3*h);
Emu04=exp(-freq*4*h);
Emu05=exp(-freq*5*h);
Emu06=exp(-freq*6*h);
Emu07=exp(-freq*7*h);
Emu08=exp(-freq*8*h);
EMU=exp(-freq*Up);%%%% Exp(-kz)
ff0=(fft2(GG6,m,n));
UC0=real(ifft2(ff0.*EMU,m,n));%%%%% Upward continue gravity anomalies at level d
ff=fft2(UC0,m,n);
UC8=real(ifft2(ff.*Emu08,m,n));%%%%%%% Upward Continuation at level 8h
UC7=real(ifft2(ff.*Emu07,m,n));%%%%%%% Upward Continuation at level 7h
UC6=real(ifft2(ff.*Emu06,m,n));%%%%%%% Upward Continuation at level 6h
UC5=real(ifft2(ff.*Emu05,m,n));%%%%%%% Upward Continuation at level 5h
UC4=real(ifft2(ff.*Emu04,m,n));%%%%%%% Upward Continuation at level 4h
UC3=real(ifft2(ff.*Emu03,m,n));%%%%%%% Upward Continuation at level 3h
UC2=real(ifft2(ff.*Emu02,m,n));%%%%%%% Upward Continuation at level 2h
UC1=real(ifft2(ff.*Emu01,m,n));%%%%%%% Upward Continuation at level h
%%%%%%%%%%%%%%%%%%% calculating downward continue by our method with N=8
```

```
for i=1:nn
gdown=9*UC0-36*UC1+84*UC2-126*UC3+126*UC4-84*UC5+36*UC6-9*UC7+UC8;
UC8=UC7;
UC7=UC6;
UC6=UC5;
UC5=UC4;
UC4=UC3;
UC3=UC2;
UC2=UC1;
UC1=UC0;
UC0=gdown;
end
%%%%%%%%%%%%%%%%%%%%%%%%%%%%%%%%%%%
i1=0;
for i=nx/2+1:nx+nx/2
    i1=i1+1;j1=0;
    for j=ny/2+1:ny+ny/2
        j1=j1+1;
        Grav_DC(i1,j1)=gdown(i,j);
    end
end
%%%%%%%%%%%%%%%%%%%%%%%%%%%%%%%%%%%
       figure(1)
contourf(x,y,Grav_DC,20);
HH=[x1(:) y1(:) Grav_DC(:)];
save('Grav_DC1km.txt','-ascii','HH');
%%%%%%%%%%%%%%%%%%%%%%%%%%%%%%%%%%% end program
```

REFERENCES

Abedi, M., Gholami, A., & Norouzi, G. H., 2013. A stable downward continuation of airborne magnetic data: a case study for mineral prospectivity mapping in central Iran. Computers & Geosciences, 52(1), 269-280.

Achache, J., Abtout, A., & Le Mouël, J. L., 1987. The downward continuation of Magsat crustal anomaly field over Southeast Asia. Journal of Geophysical Research: Solid Earth, 92(B11), 11584-11596.

Ackerman, J., 1971. Downward continuation using the measured vertical gradient. Geophysics, 36(3), 609-612.

Blakely, R. J., 1995. Potential theory in gravity and magnetic applications. Cambridge University Press, pp 414.

Briais, A., Patriat, P., Tapponnier, P., 1993. Updated interpretation of magnetic anomalies an seafloor spreading stages in the South China Sea: implications for the tertiary tectonics of Southeast Asia. J. Geophys. Res. 98 (B4), 6299–6328.

Bullard, E., & Cooper, R., 1948. The determination of the masses necessary to produce a given gravitational field. Proceedings of the Royal Society of London. Series A, Mathematical and Physical Sciences, 194(1038), 332-347.

Clarke, G. K. C., 1969. Optimum second-derivative and downward-continuation filters. Geophysics, 34(3), 424.

Cooper, G., 2004. The stable downward continuation of potential field data. Exploration Geophysics, 35(4), 260-265.

Dean, W. C., 1958. Frequency analysis for gravity and magnetic interpretation. Geophysics, 23(1), 97.

Evjen, H. M., 1936. The place of the vertical gradient in gravitational interpretations. Geophysics, 1(1), 127-136.

Fedi, M., & Florio, G., 2002. A stable downward continuation by using the ISVD method. Geophysical Journal International, 151(1), 146–156.

Ferguson, J. F., 1988. Models of the Bouguer gravity and geologic structure at yucca flat, Nevada. Geophysics, 53(2), 231-244.

Huchon, P., Hguyen, T.N.H., Chamot-Rooke, N., 2001. Propagation of continental break-up in the southwestern South China Sea. Geol. Soc., Lond., Spec. Publ. 187, 31–35.

Huestis, S. P., & Parker, R. L., 1979. Upward and downward continuation as inverse problems. Geophysical Journal International, 57(1), 171-188.

Hughes, D. S., 1942. The analytic basis of gravity interpretation. Geophysics, 7(2), 169-178.

Juan H. H. and Kevin L. M., 2002. Hilbert transform of gravity gradient profiles: Special cases of the general gravity – gradient tensor in the Fourier transform domain. Geophysics Vol. 67, No. 3, p 766-769.

Li, C.F., Xu, X., Lin, J., Sun, Z., Zhu, J., Yao, Y.J., Zhao, X.X., Liu, Q.S., Kulhanek, D.K., Wang, J., Song, T.R., Zhao, J.F., Qiu, N., Guan, Y., Zhou, Z., Williams, T., Bao, R., Briais, A., Brown, E., Chen, Y., Clift, P., Colwell., F., Dadd, K., Ding, W., Almeida, I., Huang, X., Hyun, S., Jiang, T., Koppers, A., Li, Q., Liu, C., Liu, Z., Nagai, R., Peleo-Alampay, A., Su, X., Tejada, M., Trhnh, H., Yeh, Y., Zhang, C., Zhang,F., Zhang, G., 2014. Ages and magnetic structures of the South China Sea constrained by deep tow magnetic surveys and IODP Expeition 349. Geochem., Geophys., Geosyst., 15:4958–4983. doi:10.1002/2014gc005567.

Li, L., Clift, P., Nguyen, H.T., 2013. The sedimentary, magmatic and tectonic evolution of the southwestern South China Sea revealed by seismic stratigraphic analysis. Mar. Geophys. Res. 34, 341–365.

Lima, E. A., Weiss, B. P., Baratchart, L., Hardin, D. P., & Saff, E. B., 2013. Fast inversion of magnetic field maps of unidirectional planar geological magnetization. Journal of Geophysical Research: Solid Earth, 118(6), 2723-2752.

Mansi, A. H., Capponi, M., & Sampietro, D., 2018. Downward continuation of airborne gravity data by means of the change of boundary approach. Pure and Applied Geophysics, 175(3), 977-988.

Mastellone, D., Fedi, M., Ialongo, S., & Paoletti, V., 2013. Volume continuation of potential fields from the minimum-length solution: An optimal tool for continuation through general surfaces. Seg Meeting (Vol.111, pp.346-355).

Morgan, J. P., & Blackman, D. K., 1993. Inversion of combined gravity and bathymetry data for crustal structure: A prescription for downward continuation. Earth and planetary science letters, 119(1-2), 167-179.

Nguyen N.T., S.M. Lee, and B.C. Que, 2004. Satellite gravity anomalies and their correlation with the major tectonic features in the South China Sea, *Gondwana*, *Res*. **7**, 2, 407-424, DOI: 10.1016/S1342-937X(05)70793-0.

Novák, P., Kern, M., & Schwarz, K. P., 2001. Numerical studies on the harmonic downward continuation of band-limited airborne gravity. Studia Geophysica et Geodaetica, 45(4), 327-345.

Parker, R. L., 1977. Understanding inverse theory. Annual Review of Earth and Planetary Sciences 5, 35–64.

Pašteka R., Karcol R., Kušnirák D., & Mojzeš A., 2012. Regcont: a matlab based program for stable downward continuation of geophysical potential fields using Tikhonov regularization. Computers & Geosciences, 49(4), 278-289.

Pawlowski, R. S., 1995. Preferential continuation for potential-field anomaly enhancement. Geophysics, 60(2), 390-398.

Peters, L. J., 1949. The direct approach to magnetic interpretation and its practical application. Geophysics, 14(3), 290-320.

Ramadass, G., Arunkumar, I., Rao, S.M.V., Mqhan N. L. and Sundararajan, 1987. Auxiliary functions of the Hilbert transform in the study of gravity anomalies. Proc, Indian Acad. Sci. (Earth Planet. Sci.), Vol. t)6, No. 3, December 198'7, pp. 211-219. https://doi.org/10.1007/BF02841613.

Sandwell, D.T., R. Dietmar Müller, Walter H. F. Smith, Emmanuel Garcia, Richard Francis, 2014. New global marine gravity model from CryoSat-2 and Jason-1 reveals buried tectonic structure. *Science* 346, 65 (2014) DOI: 10.1126/science.1258213.

Sandwell, D. T., E. Garcia, K. Soofi, P. Wessel, and W. H. F. Smith, 2013. Towards 1 mGal Global Marine Gravity from CryoSat-2, Envisat, and Jason-1, The Leading Edge, 32(8), 892-899. doi: 10.1190/tle32080892.1

Sandwell, D.T., and W.H.F. Smith, 2009. Global marine gravity from retracked Geosat and ERS1 altimetry: Ridge Segmentation versus spreading rate, *J. Geophys. Res*. **114**, B01411, DOI: 10.1029/2008JB006008.

Sansó F., Capponi M., Sampietro D., 2018. Up and Down Through the Gravity Field. In: Freeden W., Rummel R. (eds) Handbuch der Geodäsie. Springer Reference Naturwissenschaften. Springer Spektrum, Berlin, Heidelberg https://doi.org/10.1007/978-3-662-46900-2_93-1

Sebera, J., Pitoňák, M., Hamáčková, E., & Novák, P. 2015. Comparative study of the spherical downward continuation. Surveys in Geophysics, 36(2), 253-267.

Sebera, J., Šprlák, M., Novák, P., Bezděk, A., & Vaľko, M. 2014. Iterative spherical downward continuation applied to magnetic and gravitational data from satellite. Surveys in Geophysics, 35(4), 941-958.

Tikhonov, A. N., Arsenin, V. I., & John, F. 1977. Solutions of ill-posed problems (Vol. 14). Washington, DC: Winston.

Tomoda, Y., & Aki, K., 1955. Use of the function sin x/x in gravity problems. Proceedings of the Japan Academy, 31(7), 443-448.

Trejo, C. A., 1954. A note on downward continuation of gravity. Geophysics, 19(1), 71-75.

Tsuboi, C., & Fuchida, T., 1937. Relation between gravity anomalies and corresponding subterranean mass distribution, 1. Bull. Earthquake Res. Inst., Tokyo Univ., 15, 636-649.

Xu, S. Z., Yang, J., Yang, C., Xiao, P., Chen, S., & Guo, Z., 2007. The iteration method for downward continuation of a potential field from a horizontal plane. Geophysical Prospecting, 55(55), 883-889.

Zeng, X., Li, X., Su, J., Liu, D., & Zou, H. 2013. An adaptive iterative method for downward continuation of potential-field data from a horizontal plane. Geophysics, 78(4), 43-J52.

Zeng, X., Liu, D., Li, X., Chen, D., & Niu, C., 2014. An improved regularized downward continuation of potential field data. Journal of Applied Geophysics, 106(7), 114-118.

Zhang, H., Ravat, D., & Hu, X., 2013. An improved and stable downward continuation of potential field data: The truncated Taylor series iterative downward continuation method. Geophysics, 78(5), J75-J86.

Zhang, Y., Wong, Y. S., & Lin, Y., 2016. Bttb–rrcg method for downward continuation of potential field data. Journal of Applied Geophysics, 126, 74-86.

Zhang, C., Lü, Q., Yan, J., & Qi, G., 2018. Numerical solutions of the mean-value theorem: New methods for downward continuation of potential fields. *Geophysical Research Letters*, 45, 3461– 3470. https://doi.org/10.1002/2018GL076995

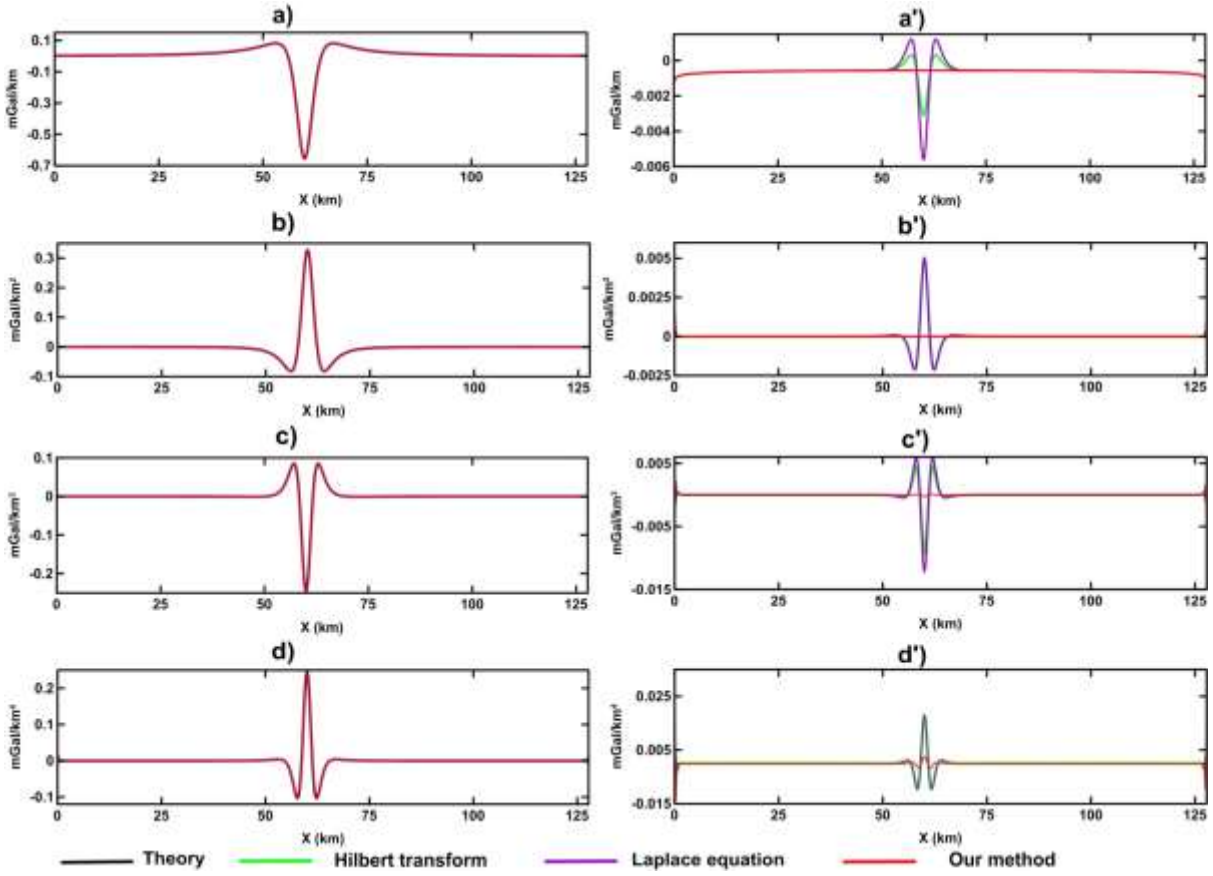

Fig. 1. VD of gravity anomaly of the infinite horizontal cylinder are calculated by Hilbert transform method (green line), Laplace equation method (purple line) and our method (red line) compared to theoretical VD (black line); a) First VD; b) Second VD; c) Third VD; d) Fourth VD; a') RMS errors of the first VD; b') RMS errors of the second VD; c') RMS errors of the third VD; d') RMS errors of the fourth VD.

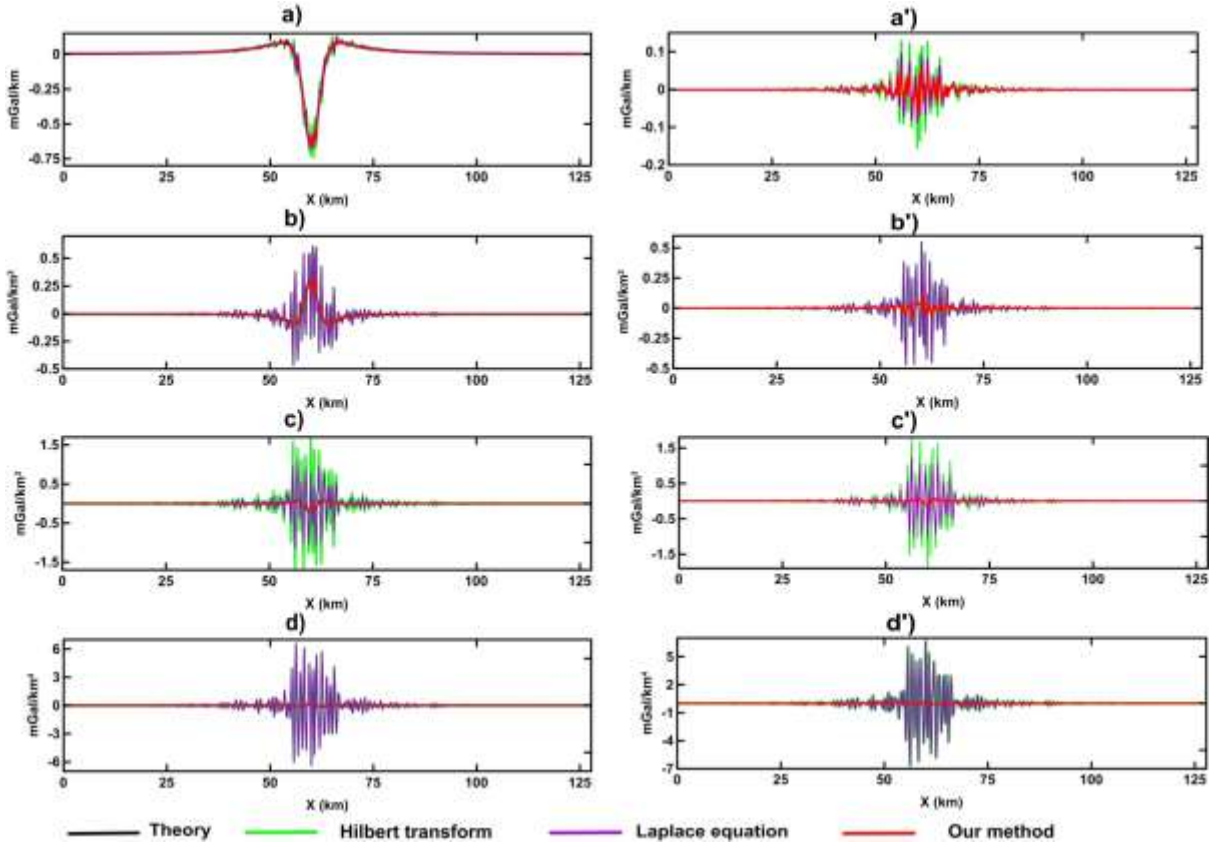

Fig. 2. VD of 5% random noise gravity anomaly of the infinite horizontal cylinder are calculated by Hilbert transform method (green line), Laplace equation method (purple line) and our method (red line) compared to theoretical VD (black line); a) First VD; b) Second VD; c) Third VD; d) Fourth VD a') RMS errors of the first VD; b') RMS errors of the second VD; c') RMS errors of the third VD; d') RMS errors of the fourth VD. (Δh=0.5 km).

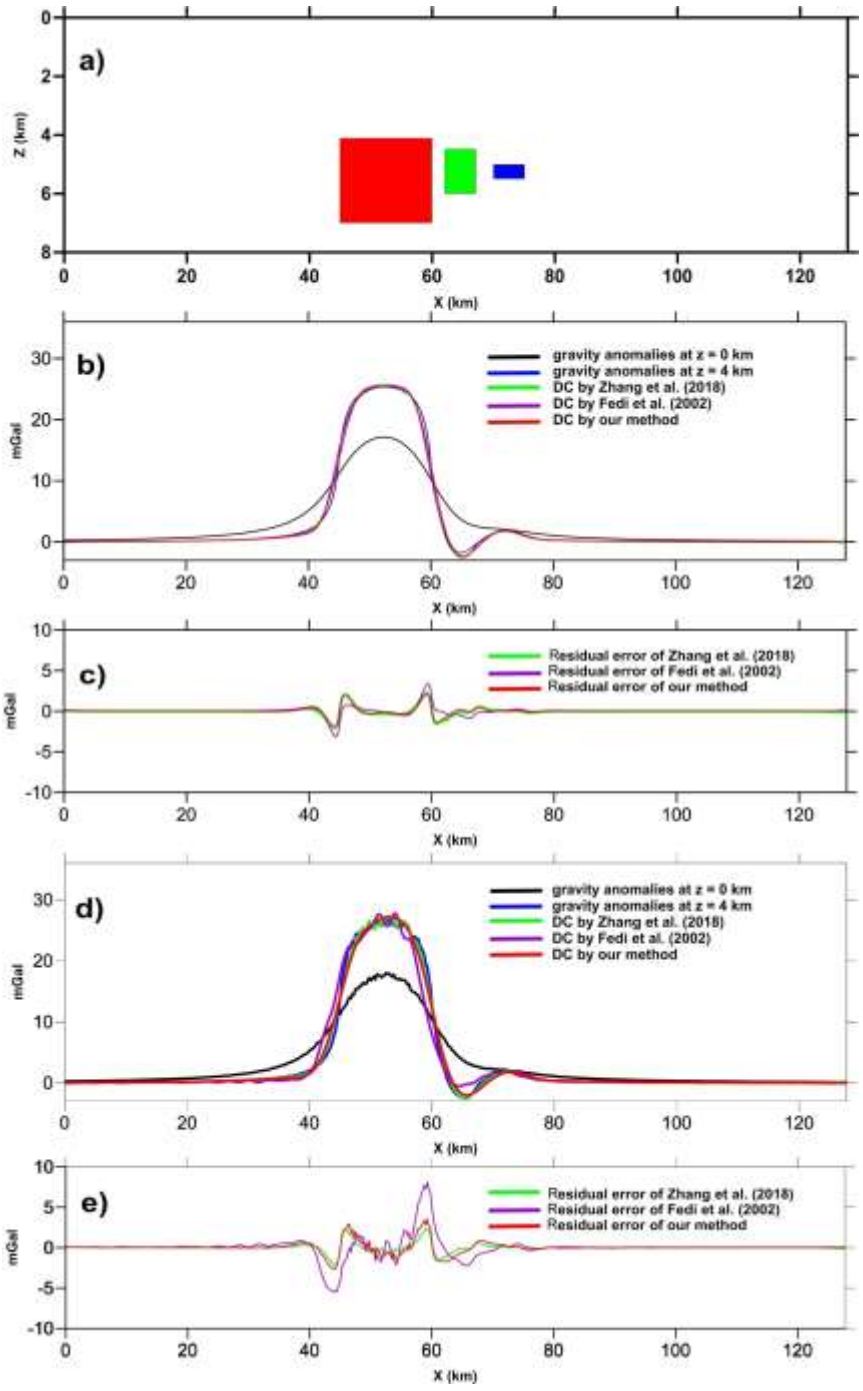

Fig. 3. a) Synthetic model of three rectangular bodies with the geometric parameters given in Table 5; b) synthetic gravity anomalies at z = 0 km (black line) and z = 4 km (blue line) without noise. The downward continuation (DC) at z = 4 km is calculated by our method (red line), Zhang et al.'s method (green line), and Fedi et al.'s method (violet line); c) Residual

errors between our method (red line), Zhang et al.'s method (green line) and Fedi et al.'s method and synthetic gravity anomalies. d) theoretical gravity anomalies at z = 0 km and z = 4 km are due to the 5% added noise (black and blue lines, respectively); red, green and violet lines represent downward continuation at z = 4 km by our method, Zhang et al.'s method and Fedi et al.'s method, respectively; e) Residual errors between our method (red line), Zhang et al.'s method (green line) and Fedi et al.'s method and synthetic gravity anomalies.

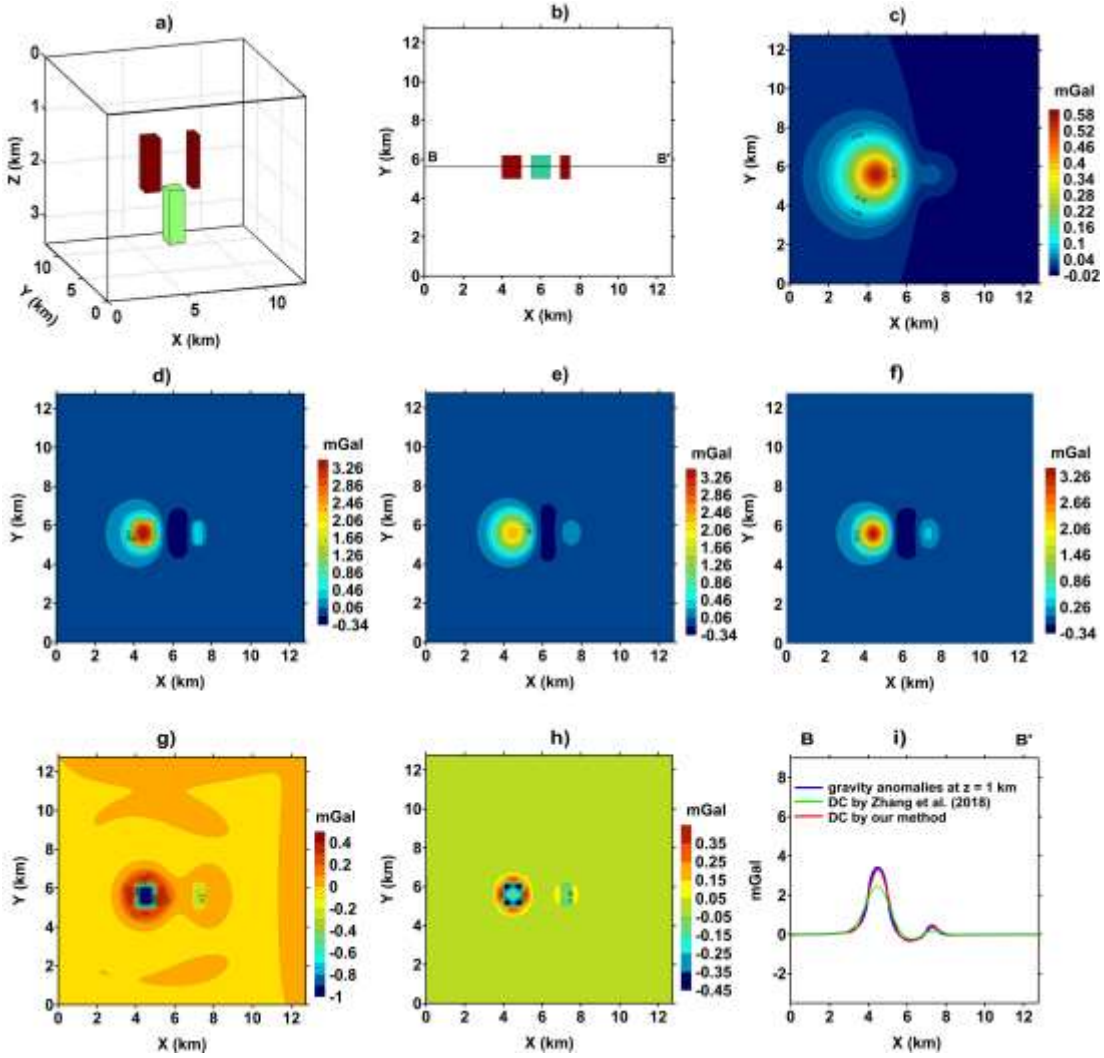

Fig. 4. 3D synthetic model of the three prisms. a) underground geological bodies; b) illustration of the model on a horizontal plane and the location of section BB'; c) theoretical gravity anomalies at z = 0 km; d) theoretical gravity anomalies at z = 1 km; e) downward continuation of (c) to 1 km by Zhang's method (Zhang et el., 2018); f) downward continuation of (c) at z = 1 km by our method; g) Residual errors between (e) and (d); h) Residual errors between (f) and (d); i) BB' section displaying theoretical gravity anomalies at z = 1 km (green line), downward continuation at z = 1 km by our method (red line), and downward continuation at z = 1 km by Zhang et at. 's method (blue line).

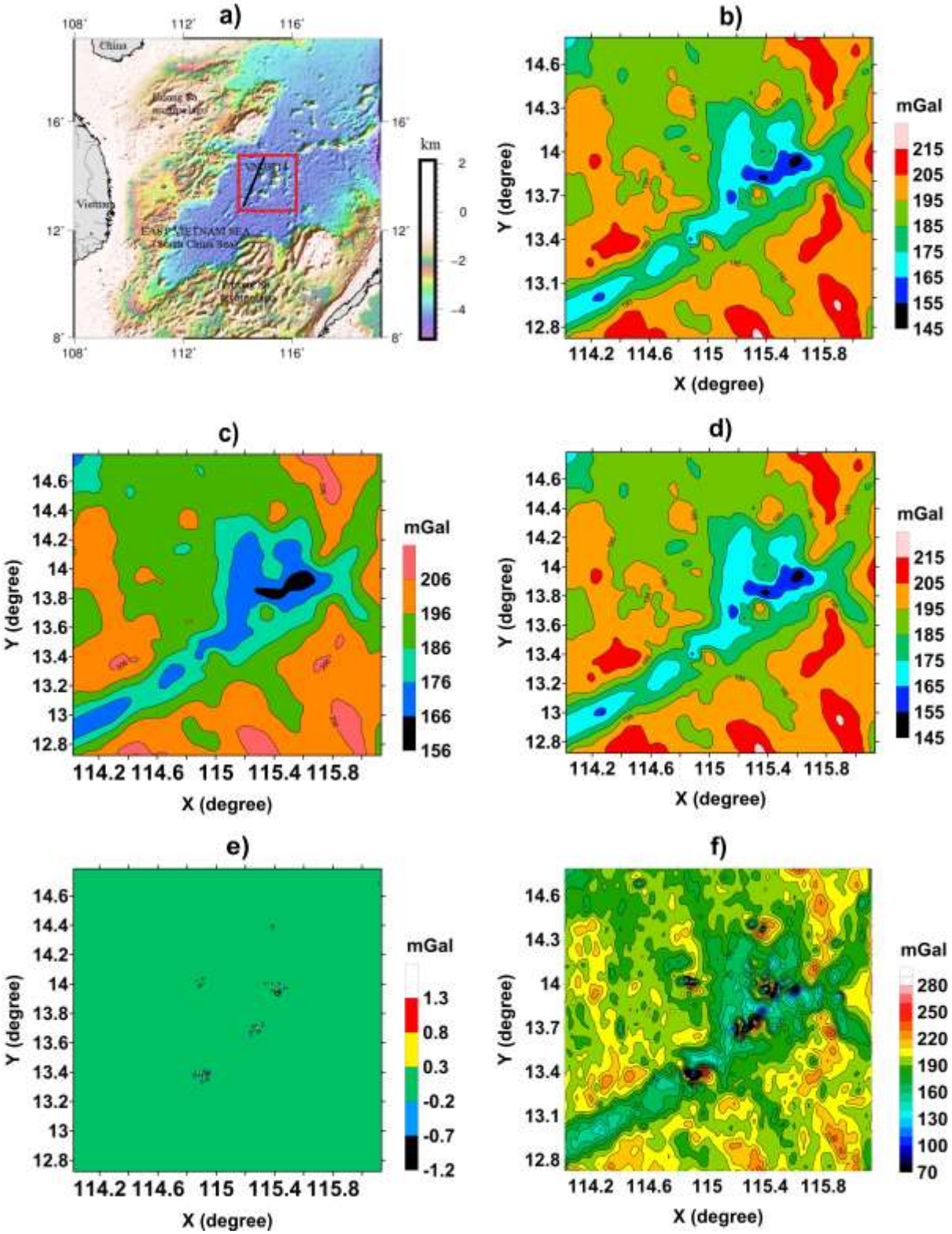

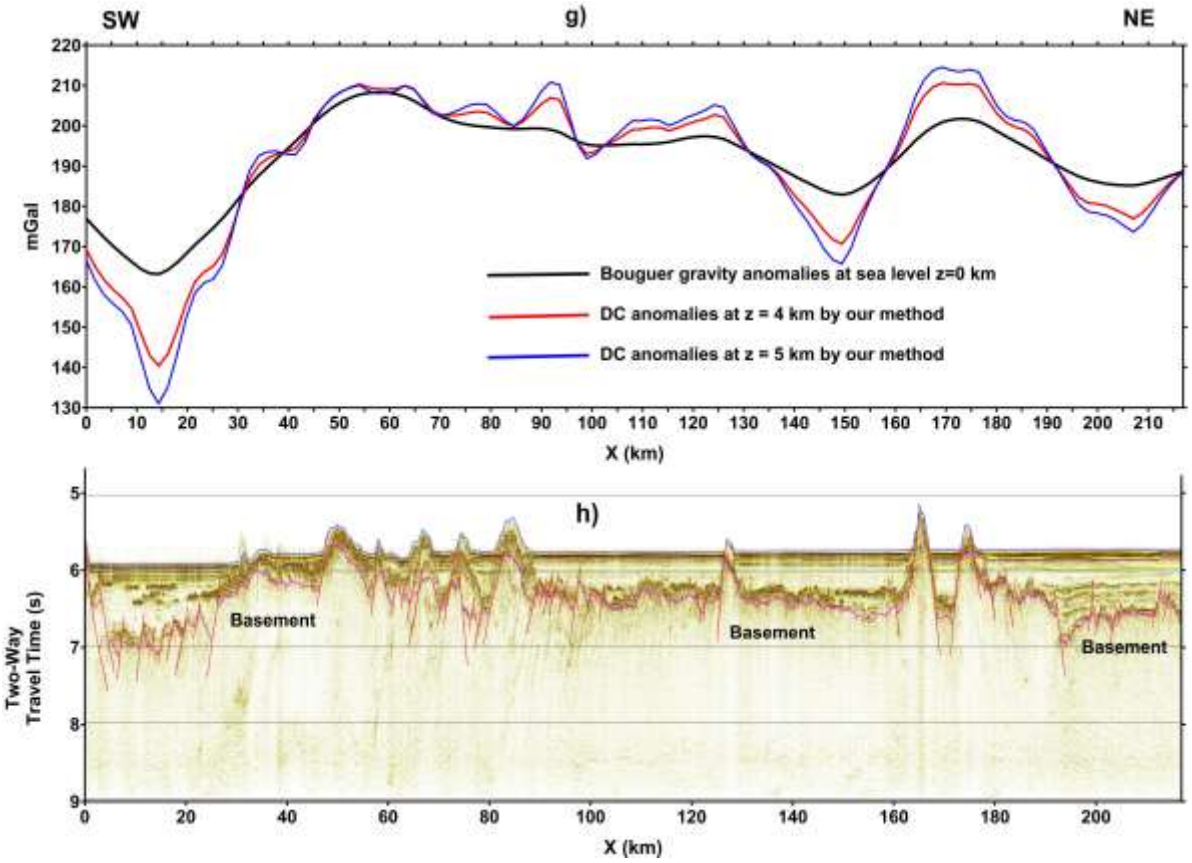

Fig 5. a) Bathymetric map, location of the study area (red square), and seismic section VN08-14 (black line); b) Satellite Bouguer gravity anomalies at sea surface (z = 0 km); c) Upward continuation of (b) at z = 4 km by FFT method; d) Downward continuation of (b) at z = 0 km (sea surface) by our method; (e) The residual error between (d) and (b); f) Downward continuation of (c) at z = 4 km by our method; g) Gravity anomalies on sea surface (black line), at z = 4 km (red line) and z = 5 km (green line); h) The seismic section VN08-14 (location in Fig. 5a).

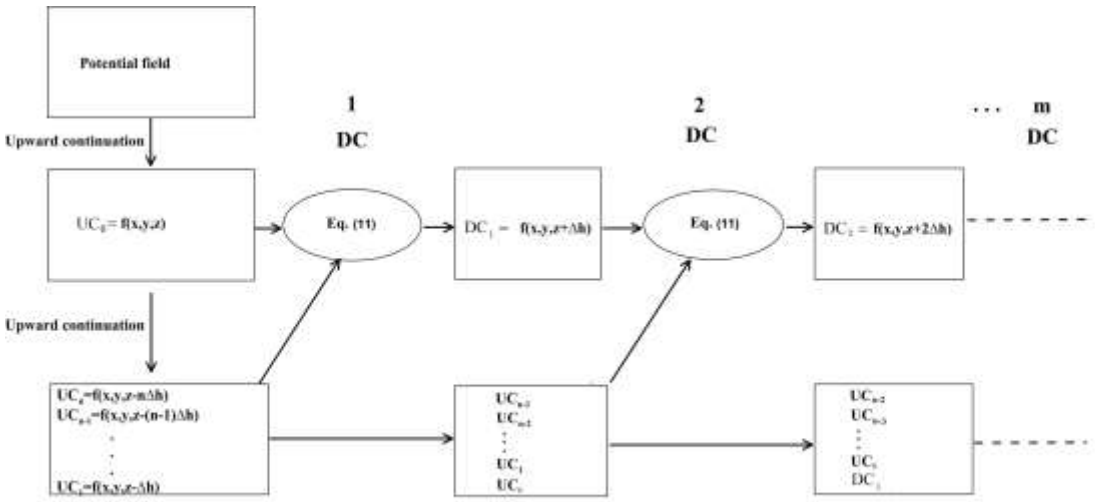

Figure B1: Calculation diagram of Downward continuation

Table 1. Obtained values a_0, a_1, ..., a_n in Equation (4) in cases of n=3, 5, 8, and 10

N	a_0	a_1	a_2	a_3	a_4	a_5	a_6	a_7	a_8	a_9	a_{10}
3	4	-6	4	-1							
5	6	-15	20	-15	6	-1					
8	9	-36	84	-126	126	-84	36	-9	1		
10	11	-55	165	-330	462	-462	330	-165	55	-11	1

Table 2: RMS errors of the VD are calculated by Hilbert transform method, Laplace equation method and our method

Calculation method	Error of first VD (mGal/km)	Error of second VD (mGal/km^2)	Error of third VD (mGal/km^3)	Error of fourth VD (mGal/km^4)
Hilbert transform	$6.8913\ 10^{-4}$	$5.8734\ 10^{-4}$	$10.3082\ 10^{-4}$	$19.441\ 10^{-4}$
Laplace equation	$8.7794\ 10^{-4}$	$5.8734\ 10^{-4}$	$13.5626\ 10^{-4}$	$19.44\ 10^{-4}$
Our method	$6.12\ 10^{-4}$	$0.79\ 10^{-4}$	$3.4753\ 10^{-4}$	$16.0053\ 10^{-4}$

Table 3: RMS errors of the VD calculated by Hilbert transform method, Laplace equation method and our method (in case, added 5% random noise to input data)

Calculation method	Error of first VD (mGal/km)	Error of second VD (mGal/km^2)	Error of third VD (mGal/km^3)	Error of fourth VD (mGal/km^4)
Hilbert Transform	$2.1874\ 10^{-2}$	$7.7909\ 10^{-2}$	$28.1046\ 10^{-2}$	$103.7828\ 10^{-2}$
Laplace's equation	$1.3654\ 10^{-2}$	$7.7909\ 10^{-2}$	$18.0075\ 10^{-2}$	$103.7828\ 10^{-2}$
Our method	$0.9603\ 10^{-2}$	$1.261\ 10^{-2}$	$1.6013\ 10^{-2}$	$2.2058\ 10^{-2}$

Table 4. RMS errors of VD when the input data were upward continued before calculating VD (in case, added 5% random noise to input data)

Calculation Method	Error of first VD (mGal/km)	Error of second VD (mGal/km^2)	Error of third VD (mGal/km^3)	Error of fourth VD (mGal/km^4)
Our method	$0.3577\ 10^{-2}$	$0.5524\ 10^{-2}$	$0.9225\ 10^{-2}$	$1.5802\ 10^{-2}$

Table 5. Geometric and density contrast parameters of 2D synthetic model

Model	x_1 (km)	x_2 (km)	z_1 (km)	z_2 (km)	Density contrast (g/cm^3)
Body 1	45	60	4.1	7	0.240
Body 2	62	67	4.5	6	-0.100
Body 3	70	75	5	5.5	0.100

Table 6: RMS error between DC gravity anomalies of our method, Zhang et al.'s and Fedi et al.'s methods and synthetic gravity anomalies

N	Downward Continuation by	RMS errors (mGal) (without noise)	RMS errors (mGal) (add 5% random noise)
1	Zhang et al., 2018	0.2072	0.224
2	Fedi et al., 2002	0.204	1.92
3	Our method	0.11	0.32

Table 7. Geometric and density contrast parameters of the 3D synthetic model

Model	X_1 *(km)*	X_2 *(km)*	Y_1 *(km)*	Y_2 *(km)*	Z_1 *(km)*	Z_2 *(km)*	*Density contrast* ρ *(g/cm^3)*
Prism 1	*4*	*5*	*5*	*6.2*	*1.01*	*2*	*0.2*
Prism 2	*5.5*	*6.5*	*5*	*6.2*	*2*	*3*	*-0.15*
Prism 3	*7*	*7.5*	*5*	*6.2*	*1.01*	*2*	*0.05*